*Annals of Biomedical Engineering*, Vol. 26, pp. 597–607, 1998
Printed in the USA. 

0090-6964/98 $10.50 + .00


# A Novel Interpolation Method for Electric Potential Fields in the Heart during Excitation

QUAN NI, ROBERT S. MACLEOD, ROBERT L. LUX, AND BRUNO TACCARDI

Nora Eccles Harrison Cardiovascular Research and Training Institute, University of Utah, Salt Lake City, UT

*(Received 24 April 1997; accepted 11 December 1997)*

**Abstract—**In mapping the electrical activity of the heart, interpolation of electric potentials plays two important roles. First, it permits the estimation of potentials in regions that could not be sampled or where signal quality was poor, and second, it supports the construction of isopotential lines and surfaces for visualization. The difficulty in developing robust interpolation techniques for cardiac applications lies in the abrupt change in potential in the vicinity of the activation wave front. Despite the resulting nonlinearities in spatial potential distributions, simple linear interpolation methods are the current standard and the resulting errors due to aliasing can be large if electrode spacing does not lie on the order of 0.5–2 mm—the thickness of the activation wave front. We have developed a novel interpolation method that is based on two observations specific to the spread of excitation in the heart: (1) that propagation velocity changes smoothly within a region large enough to contain several measurement electrodes and (2) that electrogram morphology varies very little in the neighborhood of each sample point except for a time shift in the potential wave forms. The resulting interpolation scheme breaks the interpolation of one highly nonlinear variable—extracellular potential—into two separate interpolations of variables with much less drastic spatial variation—activation time and electrogram morphology. We have applied this method to potentials originally recorded at 1.5 mm spacing and then subsampled at a range of densities for testing of the interpolation. The results based both on reconstruction of isopotential contour maps and statistical comparison showed significant improvement of this novel approach over standard linear techniques. The applications of the new method include improved determination of electrophysiological parameters such as spatial gradients of potential and the path of cardiac activation and recovery, estimation of electrograms at desired locations, and visualization of electric potential distributions. © *1998 Biomedical Engineering Society.* [S0090-6964(98)00604-3]

**Keywords—**Electrocardiography, Cardiac mapping, Activation.

## INTRODUCTION

Electric potentials measured from the cardiac surface and within the myocardium provide direct information about the electrical activity of the heart and are the basis of a great deal of what we know about macroscopic cardiac electrophysiology.[3,24,32] While more remote—and more easily obtained—electrocardiographic body-surface leads provide useful temporal information, using multiple electrodes at the heart offers much greater spatial detail, superior signal quality, and vastly improved reconstruction of three-dimensional fields. Among other advances, cardiac mapping has enabled the investigation of fundamental principles of electrocardiology such as the relation between the structure of myocardial fibers and the spread of excitation,[24,32] the effect of ischemia on propagation and recovery,[18] and the nature of reentrant arrhythmias.[29] Clinically, cardiac mapping provides information for diagnosis and treatment,[13,26] as well as for the exploration of cardiac defibrillation.[10,17]

Of great practical concern in cardiac mapping is the trade-off between spatial sampling density and coverage, the limits of which are defined by the finite number of channels that can be sampled synchronously. In a typical mapping scheme, either a large portion of the heart is explored at relatively low resolution (centimeters between electrodes) or resolution is increased to the order of millimeters, but coverage is restricted to a region of only a few square (or cubic) centimeters. The former case is inadequate for accurate measurement of local features such as conduction velocity, potential gradient or breakthrough sites, while the latter limits the ability to detect larger scale phenomena such as reentrant circuits. Even if there were no limits on the recording system itself, the number of sampling locations would still be restricted by physical access to portions of the preparation and the impact of the recording electrodes on the viability and stability of the preparation itself—especially when measuring within the myocardial wall.

As with any sampling technique, cardiac mapping relies on interpolation to reconstruct a continuous description of potential fields from discrete samples, e.g., isopotential contour maps. The generation of iso-value maps can be separated into two stages: (1) estimating values at desired locations based on recordings made elsewhere and (2) displaying the results by drawing contour lines

Address for correspondence and reprints: Robert S. Macleod, Nora Eccles Harrison CVRTI, Building 500, University of Utah, Salt Lake City, UT 84112. Electronic mail: macleod@cvrti.utah.edu

that connect locations with the same value. The core of both stages is interpolation. In the first stage, interpolation is used to fill in regions of low sampling density, to replace unusable signals, or to convert unevenly spaced data points to a regularly spaced orthogonal grid.[7] In the second stage, some form of interpolation is implicitly required to draw iso-value lines.

Few publications have addressed specifically the use of interpolation with potentials from the epicardial surface or from the volume of the heart muscle,[4,9] focusing instead on the interpolation of electrocardiograms (ECGs) for body surface potential mapping (BSPM).[4,20–22,27] The difficulty in developing robust interpolation techniques for cardiac signals lies in the abrupt change in potential in the vicinity of the activation wave front. On the body surface, in contrast, the smoothing effect of the torso volume conductor reduces both potential amplitudes and spatial gradients due to superposition of extracardiac fields from the distributed cardiac sources.[25] Despite this difference, researchers have traditionally used the same interpolation methods for cardiac potentials as those developed for BSPM and either accepted the resulting distortion or sampled with high enough spatial density to facilitate adequate interpolation. A more general weakness in applying standard techniques to interpolation of cardiac electrograms is the finding that completely *general purpose* interpolation schemes of two and more dimensions are very limited in most practical cases.[1] More fruitful are likely to be interpolation schemes that are specific and tailored to the nature of the underlying phenomena generating the signals.

We have developed such an interpolation approach that is based on two observations specific to the spread of excitation in the heart: (1) that propagation velocity changes smoothly within a region we will consider ''local'' and (2) that electrogram morphology, at least under normal conditions, varies relatively modestly in the neighborhood of each sample point except for a time shift in the potential wave forms. We propose an interpolation scheme that makes use of these findings by breaking the interpolation of one highly nonlinear variable—extracellular potential—into two separate interpolations of variables with much less drastic spatial variation—activation time and electrogram morphology. In this scheme, first activation time at a desired location is estimated by interpolating from neighboring measurement locations, based on an assumption of constant local propagation velocity. Then the wave form at the desired location is estimated through the interpolation of neighboring measured signals that have been time aligned according to the estimated activation time. This approach makes better use of all the available information than traditional methods and avoids directly interpolating a nonlinearly distributed variable. We present here the details of the method, a description of its implementation and validation, and results that demonstrate a significant improvement of this novel approach over standard techniques.

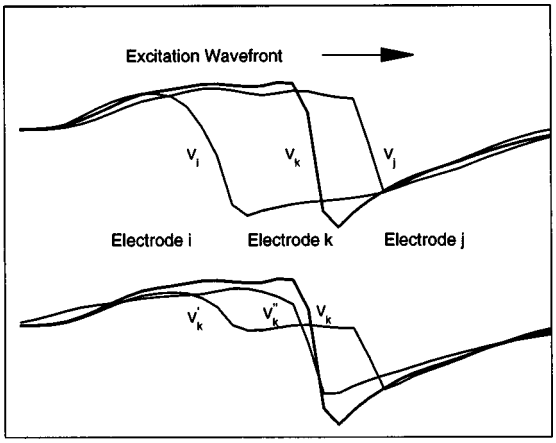


**FIGURE 1. An illustrated comparison of standard linear and wave-equation based interpolation. In upper panel, an excitation wave front travels from location *i* past location *k*, to a third location *j*, and their correspondent measured wave forms are $V_i$, $V_j$ and $V_k$. Lower panel shows estimated wave form at *k*, $V'_k(t)$, by standard linear interpolation, and $V''_k(t)$, by wave-equation based interpolation.**

## METHODS

### *Basis of the Interpolation Algorithm*

The voltage $V(x,t)$ recorded by an electrocardiographic lead is a function of space and time. Traditional interpolation methods for cardiac mapping have been based solely on spatial variables. As an example, we apply one-dimensional linear interpolation to the collinear locations $i$, $j$, and $k$ with $k$ lying between $i$ and $j$ (see Figure 1). If the wave form measured at $i$ is $V_i(t)$ and at $j$ is $V_j(t)$, the distance between $i$ and $k$ is $a$, and the distance between $k$ and $j$ is $b$, then the wave form at $k$, $V_k(t)$ can be estimated as

$$V_k(t) = \frac{b}{a+b} V_i(t) + \frac{a}{a+b} V_j(t). \qquad (1)$$

The potential distribution at any instant during activation in the heart is characterized by two adjacent, irregular regions, one containing cells at rest and a second region containing cells in an activated, depolarized state—with only millimeters of space between them. The resulting potential field is highly nonlinear and one consequence is that linear interpolation or other methods based solely on spatial variables are likely to perform poorly. However, if we consider the spread of activation as a space-time behavior that exhibits steady and uniform

propagation, then $V(x,t)$ must satisfy a wave equation of the form

$$V(x,t)=V(x-\theta t), \tag{2}$$

where $\theta$ is the propagation velocity. The implication of Equation (2) is that the wave form at any one position is similar in shape to that of neighboring sites except for a time shift. Equation (2) was actually used by Hodgkin and Huxley for deriving action potential wave forms in nerve.[15]

While cardiac spread of activation is too complex to be described as uniform and steady propagation, we may still use the notion of a wave equation applied in small local regions and incorporate it into a practical interpolation scheme that we have called wave-equation based (WEB) interpolation. Under normal conditions, each unipolar electrogram usually displays a common feature—a sharp down-stroke in the wave form—which indicates the passage of the activation wave front across the sensing electrode and marks the activation time. The signals used for interpolation are first shifted in time so that they all align according to their activation times, then spatial interpolation of the wave form is applied to the time-aligned signals. This process in our one-dimensional example can be expressed as

$$V_k(t)=\frac{b}{a+b}V_i(t+a/\theta)+\frac{a}{a+b}V_j(t-b/\theta), \tag{3}$$

where $a/\theta$ and $b/\theta$ are the times required for an excitation wave front to travel from $i$ to $k$ and from $k$ to $j$, respectively. Propagation velocity $\theta$ can be determined from activation times at $i$ and $j$, $t_i$ and $t_j$, respectively, as

$$\theta=\frac{a+b}{t_j-t_i}. \tag{4}$$

The comparison of standard linear and wave-equation based interpolation methods is illustrated in Figure 1. Due to the time displacement of the intrinsic deflection between $V_i(t)$ and $V_j(t)$, the wave form $V'_k(t)$ computed by simple linear interpolation is seriously distorted near the intrinsic deflection. The same result was observed by Blanchard *et al.*,[9] who found that linear interpolation performed better between points that lay along the cardiac fiber orientation than across the fiber. This may be explained by the fact that more rapid propagation along fibers results in smaller shifts between activation times at the measured sites—and hence smaller interpolation errors—than between sites arranged the same distance apart across fibers. One solution to this problem is to apply wave-equation based interpolation as shown in Figure 1. The measured wave forms are first time aligned and the resulting differences between interpolated wave forms become much smaller, especially during the intrinsic deflection; the resulting interpolation is substantially better, as shown by $V''_k$ in Figure 1.

### *Algorithm and Implementation*

Based on our assumption of uniform propagation in a local region, the steps required for interpolation of the potential distribution at test sites located within the mesh of measurement sites are as follows: (a) determine the activation times of all measured electrograms; (b) interpolate the activation time at test sites based on the values at their nearest neighbors; (c) for each test site, time shift the wave forms at their nearest neighbors with their activation times aligned to the interpolated activation time at the test site; and (d) interpolate the potential wave forms from the time aligned signals at the nearest neighbors. The assumption of a locally constant propagation velocity is utilized implicitly in step (b) through the linear interpolation of activation times. The assumption of similarity of wave form morphology is utilized in steps (c) and (d) for interpolation of the wave forms.

In order to apply and validate these techniques in datasets recorded from the epicardial surface, we have implemented a triangle-based linear scheme for interpolation of both activation time and wave form morphology. The algorithm can be summarized as:

(1) Triangulate the sampling locations.
(2) For any point within the mesh, first find the triangle that contains the test location and then calculate its location relative to a local Barycentric[14] coordinate system.
(3) Apply trilinear interpolation to estimate the activation time at the test location based on the values at the triangle vertices and the weighting coefficients from the Barycentric coordinates.
(4) Shift the wave forms recorded at all three vertices such that their activation times align to the interpolated activation time at the test location.
(5) Apply trilinear interpolation again to estimate the wave form at the test location from the time-aligned wave forms at the triangle vertices.

The advantages of using triangulation in our application are that (a) it supports unstructured surface grids of sampling electrodes, (b) automatic algorithms exist to generate optimal triangular connectivities for any planar distribution of points[1] (e.g., using the Voronoi diagram to create Delaunay triangularizations), and (c) the extension of the method to three-dimensional volumetric data follows directly if tetrahedra replace triangles. Linear

interpolation can provide adequate accuracy when interpolant variables do not change abruptly. Our choice of linear interpolation is not inherent to the wave-equation approach but has proved adequate for the test data described in the next section. Another feature of our scheme is that it is a *local* scheme (i.e., interpolant functions depend only on a subset of neighboring data points), which follows necessarily from the assumption of locally uniform propagation.

### *Experimental Data*

Data for testing and validation of the interpolation method came from the epicardium of exposed dog hearts. Briefly, the heart of the anesthetized, ventilated dog was exposed through a midsternal thoracotomy and suspended in a pericardial cradle. Electrode arrays were either embedded in rigid Teflon arrays or sewn into nylon stocking material with a variety of spacing and configurations. We applied the interpolation methods to recordings from six animals, and in each animal we studied propagation following both atrial pacing as well as ectopic pacing from the epicardium. Results across experiments were very consistent. In order to maintain consistency of geometry and mapping conditions, samples of interpolated potential distributions presented here are from one dog experiment in which a rigid plaque array consisting of $16\times16$ regularly spaced electrodes with 1.5 mm between adjacent centers was sutured to the right ventricular epicardium. Table 7 contains a summary of results from all six experiments recorded after atrial pacing. In all experiments, we sampled unipolar electrograms simultaneously at 1000 Hz with 12-bit resolution (by sample-and-hold) from all 256 channels. Bipolar stimuli paced the right atrium, in some cases together with simultaneous pacing from various locations on the right ventricle always at a pacing interval of 400 ms. Presented here are results from supraventricular pacing (sv) and pacing at the center (central), top and bottom (north–south) and all four edges (nesw) of the plaque. Once recorded and transferred to a minicomputer for processing, data were gain corrected, windowed to a single beat, sometimes with signal-averaging of three or four beats to increase the signal-to-noise ratio, and adjusted for baseline offset. The activation time for each electrode site was estimated from the time of occurrence of the minimum time derivative in the relevant unipolar electrogram. Data visualization took the form of a single isochronal map of activation time for each beat and sequences of isopotential instant maps displayed using the program MAP3D[19] on a workstation from Silicon Graphics (Mountain View, CA).

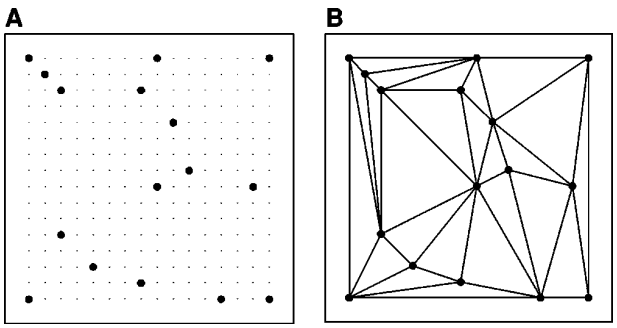


**FIGURE 2. (A) The original 16×16 sampling locations are shown as small dots and the distance between adjacent electrodes is 1.5 mm. The locations of one example of a randomly selected sub-sampling are shown as larger dots. (B) Delaunay triangulation of the sub-sampled points.**

### *Validation of Assumptions and Interpolation Results*

We tested the assumption of constant local conduction velocity by performing linear interpolation of activation time based on subsets of the plaque electrodes [see Figure 2(A)] and comparing the results to the full-resolution measurements. To evaluate the effect of sampling location, we used both regularly spaced and randomly generated sub-samplings for this test; the statistical evidence presented in Tables 1, 2, and 3 consists of mean values for 20 randomly selected sub-samplings. We took a similar approach to validation of the interpolation method by applying it to subsets of the plaque electrodes and comparing the results against original recordings. In both cases, reconstructed signals were compared with original recordings using correlation coefficient (CC), relative error (RE), and root-mean-square error (RMSE) computed as

$$\mathrm{CC}=\frac{\Sigma_{i=1}^{N}(V_i^m-\overline{V^m})(V_i^e-\overline{V^e})}{\sqrt{\Sigma_{i=1}^{N}(V_i^m-\overline{V^m})^2}\sqrt{\Sigma_{i=1}^{N}(V_i^e-\overline{V^e})^2}}, \tag{5}$$

$$\mathrm{RE}=\sqrt{\frac{\Sigma_{i=1}^{N}(V_i^e-V_i^m)^2}{\Sigma_{i=1}^{N}(V_i^m)^2}}, \tag{6}$$

$$\mathrm{RMSE}=\sqrt{\frac{\Sigma_{i=1}^{N}(V_i^e-V_i^m)^2}{N}}, \tag{7}$$

where $V_i^m$ represents the measured values and $V_i^e$ represents the estimated values, $N$ is the number of samples compared, $\overline{V^m}$ is the mean of the $V_i^m$'s and $\overline{V^e}$ is the mean of the $V_i^e$'s. CC can be pictured as the cosine of the angle between vectors formed by ($V_i^m$ and $V_i^e$), $i=1, \ldots, N$ and ranges between 1.0 when the vectors are colinear with the same orientation and 0 when the

**TABLE 1. Correlation coefficients between measured and interpolated activation times (mean±S.D.). $p<0.0001$ for central vs NESW and North–South vs NESW at all distances, Wilcoxon signed rank test.**

| Number of sub-samples | Ave. distance (mm) | Pacing sites | | |
|---|---|---|---|---|
| | | Central | North–South | NESW |
| 8 | 13.5 | 0.81±0.15 | 0.65±0.05 | 0.50±0.11 |
| 16 | 8.7 | 0.90±0.03 | 0.81±0.05 | 0.62±0.10 |
| 32 | 5.6 | 0.94±0.02 | 0.91±0.04 | 0.72±0.12 |
| 48 | 4.4 | 0.96±0.01 | 0.95±0.02 | 0.79±0.05 |
| 64 | 3.6 | 0.97±0.01 | 0.96±0.03 | 0.82±0.06 |

**TABLE 3. RMS errors (ms) between measured and interpolated activation times (mean±S.D.). $p<0.0001$ for central vs NESW and North–South vs NESW at all distances, Wilcoxon signed rank test.**

| Number of sub-samples | Ave. distance (mm) | Pacing sites | | |
|---|---|---|---|---|
| | | Central | North–South | NESW |
| 8 | 13.5 | 4.6±1.2 | 4.4±0.3 | 4.7±0.6 |
| 16 | 8.7 | 2.9±0.6 | 3.4±0.4 | 4.1±0.6 |
| 32 | 5.6 | 2.0±0.5 | 2.3±0.4 | 3.5±0.1 |
| 48 | 4.4 | 1.7±0.3 | 1.8±0.3 | 3.1±0.4 |
| 64 | 3.6 | 1.4±0.3 | 1.6±0.5 | 2.8±0.2 |

vectors are orthogonal and hence the signals uncorrelated. CC shows more sensitivity to differences in *pattern* than *amplitude* of the signals. The RMSE represents the average squared error between signals in absolute terms and the RE is the RMSE normalized by the mean signal power. The mean correlation coefficients, relative errors, and RMS errors were compared using one sample sign test and Wilcoxon signed rank test for paired data where appropriate. Confidence levels of 95% were considered statistically significant.

To test the assumption of similarity of morphology between wave forms in local regions, we computed the isocorrelation maps between each recorded electrogram and all other wave forms from the same beat. The result for each beat was a set of 256 isocorrelation maps, one for each site. In each map the value of 1.0 marked the site of the reference signal while isocontours connected sites of equal correlation between the reference and other electrograms. Regions with values near zero indicate signals with very low correlation to the reference.

## RESULTS

### *Interpolation of Activation Time*

We first show results from linear interpolation of the activation time in order to test one of the fundamental assumptions of the wave-equation based interpolation scheme—that within a region defined by first-order neighbors the propagation speed is relatively constant and hence the activation time varies linearly.

Figure 3 shows linearly interpolated values of activation time after pacing from a ''central'' pacing site for a series of progressively coarser regularly spaced subsamplings of the original measurement array. The original sampling locations are indicated by small dots and sub-sampling locations are indicated by larger dots on the isochronal maps. Even as the sampling resolution decreased from 1.5 mm to 7.5 mm and the number of measurement sites went from $16\times16$ to $4\times4$, isochronal lines still preserved the main features of the spread of excitation, visible both in the plots and through the statistical measures of difference between original and reconstructed activation times. For the $4\times4$ case: CC $=0.98$, RE$=1.1\%$, and RMSE$=1.5$ ms. The region surrounding the pacing site showed families of roughly elliptical isochrones reflecting continuous, anisotropic propagation from the pacing electrode with the major axis of the isochrones parallel to the fiber direction near the pacing site—all features of spread of cardiac activation that have been well documented by other experimental[23,32] and theoretical[12,23] studies.

**TABLE 2. Relative errors (%) between measured and interpolated activation times (mean±S.D.). $p<0.0001$ for central vs NESW and North–South vs NESW at all distances, Wilcoxon signed rank test.**

| Number of sub-samples | Ave. distance (mm) | Pacing sites | | |
|---|---|---|---|---|
| | | Central | North–South | NESW |
| 8 | 13.5 | 3.36±0.87 | 2.91±0.19 | 4.38±0.56 |
| 16 | 8.7 | 2.16±0.42 | 2.22±0.26 | 3.78±0.54 |
| 32 | 5.6 | 1.48±0.35 | 1.52±0.27 | 3.26±0.59 |
| 48 | 4.4 | 1.23±0.22 | 1.19±0.21 | 2.87±0.37 |
| 64 | 3.6 | 1.03±0.01 | 1.04±0.35 | 2.61±0.41 |

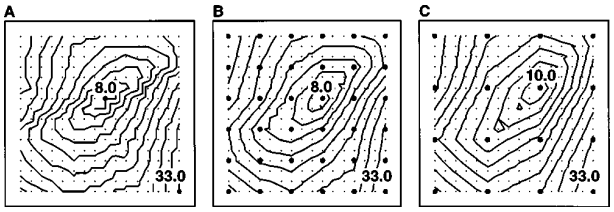


**FIGURE 3. Interpolation of activation time from measured and interpolated versions of the data. Original sampling locations are indicated by small dots and sub-sampling locations are indicated by larger dots. Interval between adjacent contour lines is 2.5 ms. The locations and times of earliest and latest activation times are marked by the text labels. (A) Isochronal map of original 16×16 recording. (B) Isochronal map of interpolated data based on a 6×6 sub-sampling. (C) Isochronal map of interpolated data based on a 4×4 sub-sampling.**

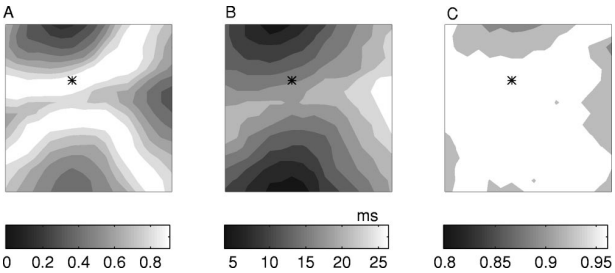


**FIGURE 4. Isocorrelation and isochrone maps from the same beat initiated by dual stimuli near the bottom and top of the plaque. (A) Isocorrelation map between the measured electrogram from electrode 118, whose location is indicated on the map by a (*) symbol, and all other electrograms recorded during the same beat. Correlations in the white area lie between 0.9 and 1. (B) Isochrone map for this beat. (C) Isocorrelation map for electrode 118 but this time calculated from time-aligned signals. Correlations in the white area lie between 0.95 and 1.**

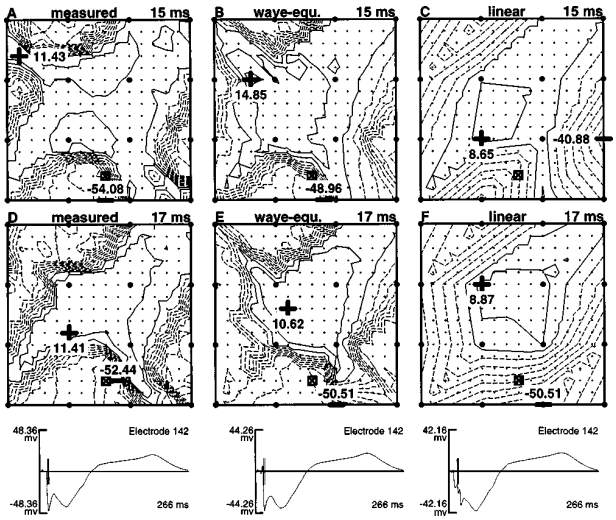


**FIGURE 5. Comparison of linear and wave equation based interpolations. Stimulus pulses were applied simultaneously at all four edges of the plaque. (A) and (D) contain isopotential maps of the original recording. (B) and (E) contain isopotential maps of the same data interpolated from a 4×4 sub-sampling grid (marked by large dots) using our wave-equation based interpolation. (C) and (F) show isopotential maps computed from the same sub-sampling mesh but using standard linear interpolation. The time instant selected for the data in the top row of panels, (A)–(C) was 15 ms after pacing while that for the middle row, (D)–(F) was 2 ms later. Both instants are marked as vertical lines in the bottom panels, which show electrograms (of 266 ms duration) measured or estimated at electrode 142, whose location is marked on the isopotential maps by the square containing the "x." Interval between adjacent contours is 6 mV. Bold "+" and "−" indicate the location of the maximum and minimum with their valued marked in each map.**

The statistical results of activation time interpolation for different pacing configurations are shown in Tables 1, 2, and 3. The tables contain means and standard deviations for each pacing site based on 20 randomly selected sub-samplings. Interpolation results from random selections of subset were not significantly different with the same pacing configuration ($p > 0.50$, one sample sign test when the number of sub-samples is more than 32). The level of interpolation errors was, however, significantly different ($p < 0.0001$, Wilcoxon signed rank test) between simple activation sequences, for example, from ''central'' or ''north–south'' pacing, and more complex activation resulting from ''NESW'' pacing, with relative errors typically 1%–2% higher in the latter case.

### *Continuity in Potential Wave Form Morphology*

A second assumption of the wave-equation based interpolation scheme is that the shapes of potential wave forms are similar in a local region except for a time shift in the signal. We tested this hypothesis by constructing isocorrelation maps between wave forms from different electrodes during the same beats and present here a single representative result from a ''north–south'' pacing experiment.

Panel (A) of Figure 4 shows the isocorrelation map for electrode 118, whose location is indicated by a (*) symbol lying within the region of maximum correlation coefficient value (CC>0.9) on the map. Panel (B) shows the isochrone map of the same activation sequence. After the electrograms were time shifted and aligned according to the activation times, correlation with electrode 118 produced the isocorrelation map in panel (C). Note first the resemblance in shape between the isocorrelation map of the unshifted data and the activation isochrone map [panels (A) and (B)], suggesting that highly correlated electrograms are those that have nearly the same activation time as the reference (electrode 118 in this case). When the timing differences were removed by shifting each electrogram according to its activation time, the correlation increased sharply and the isocorrelation map became very ''flat'' with all values in the range of 0.89–1.0.

### *Performance of the Wave-equation Based Interpolation Method*

Figures 5 and 6 show comparisons among the original, measured potentials [in the leftmost column, panels (A) and (D)] and potentials interpolated by both the wave-equation based method [middle column, panels (B) and (E)], and using standard, linear methods [rightmost column, panels (C) and (F)].

These results illustrate clearly the improvement of the wave-equation based interpolation over standard linear methods. Note, for example, the densely packed bundles of isopotential lines that identify the location of the activation wave front. In Figure 5, maps constructed from the measured potentials show in panel (A) four independent wave fronts corresponding to the pacing from four

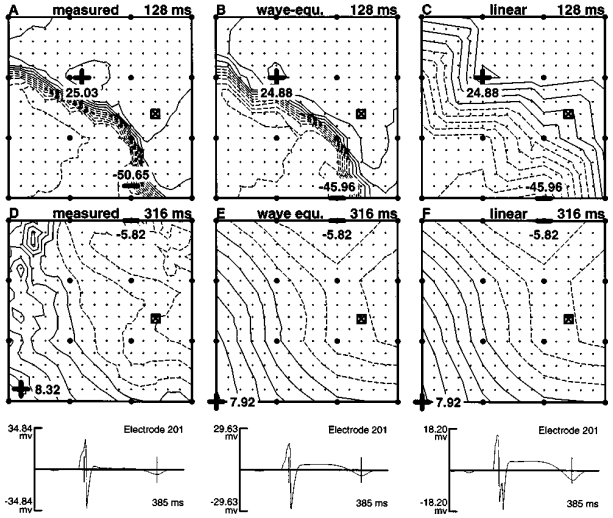


**FIGURE 6. Comparison of linear and wave equation based interpolations during supraventricular pacing. Map arrangement is the same as in Figure 5. Interval between adjacent contour lines in the maps on the top row (128 ms after pacing) is 6 mV and in the the maps on the second row (316 ms after pacing) is 1.5 mV.**

sites and in panel (D), recorded 2 ms later, a merging of wave fronts in the upper left corner to form a single, irregular boundary between depolarized and resting regions. The same information is apparent in the potentials estimated using the wave-equation based method shown in panels (B) and (E), with the extent of the merging slightly delayed in panel (E) compared to panel (D). The results of simple linear interpolation, in contrast, suggest a single, broad activation wave already in the upper panel (C) with very poor spatial localization of wave front features.

The electrograms shown in the bottom row of the figure reveal other characteristics of the interpolation. While the wave-equation based method reconstructed the electrogram shape quite well, essential features of the QRS were obliterated by simple linear interpolation and showed multiple intrinsic deflections in the time signal.

**TABLE 4. Correlation coefficients between measured and interpolated potentials. (mean±S.D.). $p<0.0001$ for linear vs wave-equation based interpolation in all cases, except for $^*p=0.004$, Wilcoxon signed rank test.**

| Pacing sites | Number of sub-samples | Ave. distance (mm) | Linear | WEB |
|---|---|---|---|---|
| Central | 4×4 | 7.5 | 0.94±0.04 | 0.97±0.04 |
| | 6×6 | 4.5 | 0.97±0.03 | 0.99±0.02 |
| North–South | 4×4 | 7.5 | 0.90±0.07 | 0.95±0.07 |
| | 6×6 | 4.5 | 0.95±0.04 | 0.98±0.02 |
| NESW | 4×4 | 7.5 | 0.89±0.08 | 0.91±0.09* |
| | 6×6 | 4.5 | 0.94±0.07 | 0.96±0.08 |

**TABLE 5. Relative errors (%) between measured and interpolated potentials. (mean±S.D.). $p<0.0001$ for linear vs wave-equation based interpolation at all cases, except for $^*p=0.0002$, Wilcoxon signed rank test.**

| Pacing sites | Number of sub-samples | Ave. distance (mm) | Linear | WEB |
|---|---|---|---|---|
| Central | 4×4 | 7.5 | 18.2±6.6 | 12.8±6.4 |
| | 6×6 | 4.5 | 13.6±5.8 | 9.1 ±5.1 |
| North-South | 4×4 | 7.5 | 25.8±1.1 | 18.4±1.4 |
| | 6×6 | 4.5 | 17.9±7.6 | 10.5±7.2 |
| NESW | 4×4 | 7.5 | 25.2±9.1 | 22.9±12.7* |
| | 6×6 | 4.5 | 17.9±8.6 | 14.4±9.9 |

The statistical results of interpolation for different pacing configurations and sub-sampling resolutions are shown in Tables 4, 5 and 6. The tables contain means and standard deviations for comparisons between QRS segments (approximately 90 frames selected on the basis of fiducials from an RMS voltage curve calculated from all electrograms) of recorded signals and interpolated estimates. Wave-equation based interpolation showed consistently better performance than simple linear interpolation in all pacing configuration ($p<0.0001$). It yielded the best results when activation patterns were simple, e.g., ''central'' pacing, which is when our assumptions are best met.

The previous results compared wave-equation based and linear interpolation methods when stimulation was applied in the neighborhood of the recording electrodes. For stimulation from a more distant site, e.g., during supraventricular pacing, wave-equation based interpolation generally still performed better (and never worse) than the linear approach for reconstructing potential distributions. In Figure 6, the top panels [(A), (B), and (C)] show isopotential contours from 128 ms after pacing at the right atrium as a wave front is passing through the recording region. While the wave-equation based interpolation constructed from a 4×4 sub-sampling grid [panel (B)] reproduced the measured wave front [panel

**TABLE 6. RMS errors (mV) between measured and interpolated potentials. (mean±S.D.). $p<0.0001$ for linear vs wave-equation based interpolation at all cases, Wilcoxon signed rank test.**

| Pacing sites | Number of sub-samples | Ave. distance (mm) | Linear | WEB |
|---|---|---|---|---|
| Central | 4×4 | 7.5 | 4.41±1.67 | 3.08±1.60 |
| | 6×6 | 4.5 | 3.28±1.36 | 2.17±1.11 |
| North-South | 4×4 | 7.5 | 5.86±1.98 | 4.01±2.40 |
| | 6×6 | 4.5 | 4.12±1.66 | 2.34±1.34 |
| NESW | 4×4 | 7.5 | 5.83±2.12 | 5.19±2.62 |
| | 6×6 | 4.5 | 4.17±2.15 | 3.30±2.35 |

**TABLE 7. Comparison between direct linear and wave-equation based (WEB) interpolation during supraventricular pacing.**

| | CC | | RE | | RMS(mV) | |
|---|---|---|---|---|---|---|
| Exp. ID | Linear | WEB | Linear | WEB | Linear | WEB |
| 1 | 0.88±0.11 | 0.92±0.12 | 0.43±0.19 | 0.33±0.21 | 5.05±2.17 | 3.87±2.41 |
| 2 | 0.95±0.07 | 0.96±0.06[a] | 0.25±0.14 | 0.23±0.13[b] | 1.88±1.10 | 1.74±1.09[c] |
| 3 | 0.92±0.10 | 0.92±0.09[d] | 0.35±0.19 | 0.34±0.19[e] | 2.61±1.40 | 2.55±1.48[f] |
| 4 | 0.90±0.12 | 0.95±0.05 | 0.35±0.19 | 0.26±0.13 | 3.33±1.72 | 2.57±1.30 |
| 5 | 0.91±0.10 | 0.93±0.10 | 0.39±0.29 | 0.34±0.29 | 2.53±1.20 | 2.14±1.14 |
| 6 | 0.85±0.20 | 0.92±0.10 | 0.42±0.26 | 0.35±0.22 | 3.30±2.14 | 2.78±1.87 |

Wilcoxon signed rank test; $p<0.0001$ for linear vs wave-equation based interpolation at all cases, except for the following.

[a] $p=0.518$.
[b] $p=0.0243$.
[c] $p=0.0249$.
[d] $p=0.5287$.
[e] $p=0.3169$.
[f] $p=0.8807$.

(A)] accurately, linear interpolation once again showed very poor spatial resolution of location, potential gradient and width of the wave front. During the recovery period, e.g., 316 ms after pacing, both interpolation methods performed equally [panels (E) and (F)].

Table 7 contains a summary of statistical results of interpolation of potentials following supraventricular pacing across all six experiments. In each case, the sub-sampling electrodes were approximately 10 mm apart. Wave-equation based interpolation showed significantly better ($p<0.0001$) performance than the linear method in four of six experiments. We note that in experiment 3, in which the wave-equation based approach had similar results to those from the linear method, the entire measurement region (about 4 cm × 5 cm) activated within only 20 ms, presumably as a result of the action of the Purkinje system. As a consequence, the isochrone map exhibited an irregular distribution suggesting deviation from our assumption of smooth local propagation.

The performance of the two interpolation methods over an entire beat is shown in Figure 7, in which we computed RMS error across all the *interpolated* locations and plotted it as a function of time. The improvement of the wave-equation based interpolation over the simple linear method was largest as the activation wave front passed under the recording electrodes (QRS), when the potential distribution showed the greatest spatial variation. During repolarization, when spatial variation was small, both methods performed equally well.

## DISCUSSION

### *Interpolation of Activation Time*

The interpolation of activation time is the first step of our interpolation technique and is based on the notion that propagation speed in normal tissue is locally constant and thus activation time varies linearly in space. At a microscopic level (<200 $\mu$m), many studies have shown that excitation in cardiac muscle spreads from cell to cell in discrete steps.[28,30] However, at a larger scale (several millimeters or greater), these discontinuities can no longer be detected. Instead, propagation velocity varies smoothly with changes in myocardial fiber orientation with the result that within a local region (millimeters to perhaps 1 cm) we can consider it to be approximately constant.[31] Our results of interpolating activation time suggest that for normal tissue with electrode spacing

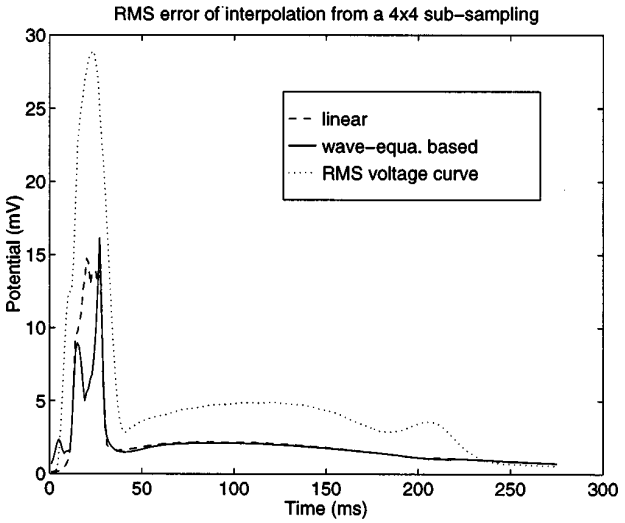


**FIGURE 7. RMS error (mV) between measured and interpolated (from a 4×4 sub-sampling) potentials during supraventricular pacing. RMS error is computed across all 240 estimated leads and plotted as a function of time. A RMS voltage curve computed from all 256 recorded electrograms is also shown as a dotted curve for time reference.**

ranging from 1.5 to 7.5 mm, this assumption is acceptable. Compliance is best when propagation is relatively simple, for example from a single stimulus site, but even for multiple site pacing resulting in collision (e.g., nesw), relative errors at 7.5 mm spacing were still within 5%. More complex and also more remote pacing leads to either the collision of multiple wave fronts or to wave fronts that impinge from below upon the epicardial surface and produce delays and accelerations of apparent propagation velocity.

### *Continuity in Potential Wave Form Morphology*

The second assumption of the wave-equation based method is that wave form morphology is relatively similar in the region between sampling electrodes and that differences in the time signals lie primarily in the time shift that reflects the movement of the activation wave front. We used a signal processing approach that is sensitive to signal morphology by computing correlation coefficients between electrograms to test this assumption. One easily recognizable feature of the resulting isocorrelation maps was their resemblance to the activation isochrone map when the reference electrode was near the site of earliest activation. The finding that sites with highly correlated wave forms are also sites with similar activation times suggests that activation time is the dominant feature determining the differences between wave shapes. From this, we suggest that by removing the differences in activation time—by aligning the wave forms—we remove a great deal of the difference between wave morphologies, and thus increase the accuracy of subsequent interpolation. The isocorrelation map constructed from *time aligned* electrograms in Figure 4 strongly supported this finding.

### *Wave-equation Based Interpolation*

We have presented here a novel approach of interpolating electric potentials in the heart during activation. While few studies have addressed interpolation of cardiac signals specifically, the difficulty clearly lies in the starkly nonlinear spatial distribution of electric potentials during activation. With the development of the wave-equation based interpolation method we attempt to utilize the relatively smoothly varying local propagation velocity and the uniformity of morphology of potential wave forms to replace interpolation of one rapidly changing variable by interpolation of two, more smoothly changing variables. This approach has shown significant improvement over traditional linear interpolation in estimating potential distributions.

The wave-equation based interpolation method gives the best results when both of the continuity assumptions are met. Even with healthy, normal tissue, there arise conditions in which epicardial activation velocity slows and then jumps again suddenly, presumably the result of wave fronts impinging on the surface at oblique angles.[31] Under such conditions, one can expect a reduction in the accuracy of the wave-equation based interpolation approach. One such example is shown by the RMS error of interpolation during supraventricular pacing in Figure 7. The wave-equation based approach produced two peaks in the error curve during the QRS, with the second peak slightly exceeding the error levels of linear interpolation. The isochrone map of the same beat shows that at the beginning and end of the QRS, the wave front propagation velocity underwent especially irregular changes, thus violating the assumption of constant propagation velocity, which in turn reduced the interpolation accuracy. This is to be expected in the case of supraventricular pacing, where epicardial sites sense wave fronts advancing from the depths of the myocardium over a range of oblique angles. In contrast, this oscillating behavior of the error was not present in cases of local stimulation (e.g., central pacing), in which the wave front traveled primarily along the epicardial surface.

We have not yet tested the method when pathological conditions would lead to abnormal conduction, and thus significant deviation from one or both assumptions. In the case of ischemia or infarct, tissue below an electrode may not support conduction of excitation, resulting in local delays or even block. Under these conditions we would expect interpolation of potentials to be problematic for both linear and wave-equations based approaches due to nonlinearities in the distributions of both potentials and activation time, as well as the ambiguities in determining activation time under such conditions.[8] However, it is certainly encouraging that even during dynamic conditions such as ventricular tachycardias, the level of correlation between signals within local regions has been shown to be useful as a metric to characterize the phenomenon.[11] This suggests that even under some extreme conditions spatial coherence of the signal morphologies is maintained. An ongoing project in our laboratories is to investigate more robust interpolation techniques that are less sensitive to the spatial gradients in the potential distributions than linear interpolation for estimating activation time and wave form morphology.

Another limitation of the method is the requirement of the unique determination of activation time from electrograms. Even though finding the minimum peak of $dv/dt$ from the unipolar electrogram has been the standard practice in determining activation time, this algorithm becomes ambiguous with electrograms that exhibit abnormalities, e.g., multiple peaks in the time derivative or slurring of the potential downslope, as discussed by Ideker *et al.* [16] However, as methods of detecting activation improve, so too will the wave-equation based approach.

The advantages of wave-equation based interpolation methods for estimating potential distribution in the heart during activation include:

(1) The individual steps of the method are each simple and fall within the usual tools available for studies of cardiac mapping; computational cost is very reasonable compared to simple linear interpolation.
(2) The interpolation steps are linear as we have implemented the method, but improvements may well be possible with more refined interpolation approaches, the topic of ongoing studies.
(3) The method can be easily expanded into three dimensions for studying electric potential distribution in the volume of the heart, which is another future research topic.
(4) The method is explicitly *not* general purpose, but instead based on features of the actual signals and could be customized to different situations in electrophysiology and even further improved as we learn more about the nature of potentials from the heart.

A subject closely related to interpolation that is implicit in our study is the minimum spatial sampling rate required to measure accurately the continuous potential distribution from discrete samples. Any theoretical discussion of such criteria will clearly be hampered for reasons similar to those suggested by Barr *et al.* in the context of temporal sampling rates:[5] (1) there is a lack of prior knowledge of the true upper frequency limit of the distributions and (2) the effect of noise in masking useful information is often unknown. A more practical approach is to define the minimum sampling rate to be the one that allows the reconstruction of continuous potential distributions with errors that are within the noise level of the measurement system. Since the spatial scale varies between different electrocardiographic phenomena, it is necessary to establish different application-specific sampling rates rather than a *general purpose* one. For example, 2 mm has been found necessary for identifying a breakthrough on ventricular surface[2] and 1 mm for examing spatial organization during ventricular fibrillation.[6]

For the purpose of testing the wave-equation based interpolation method, we have sampled at a relatively high resolution (1.5 mm between electrode centers) and then attempted to reproduce this same level of detail using interpolations based on sub-samplings at various densities. We first showed that activation time can be interpolated linearly to within relative errors of $\leqslant 3.5\%$ using a variety of irregular sampling grids with 5.6 mm average spacing even for complex stimulation patterns. Using the activation timing to align electrograms—the wave-equation based interpolation method—we achieved relative errors in potential interpolation in the range of 14% with 4.5 mm spacing. These results suggest that higher sampling density is needed to represent potential distributions than activation time and, furthermore, that sampling densities that are adequate for one activation pattern, may fail under other activation conditions. Our results do indicate that a wave-equation based approach can reduce the required sampling density and thus shift the coverage versus density trade-off in a favorable direction.

Immediate applications of this new interpolation method will be used in determining important electrophysiological parameters such as spatial gradients of cardiac potentials, estimating electrograms at desired locations, and visualizing distributions of potential. The new technique involves no more computational expense than commonly used methods. It can be easily implemented into signal quality control programs as well as visualization applications for cardiac mapping software. The successful reconstruction of complex activation situations, e.g., collision of four excitation wave fronts with modest sampling resolution (7.5 mm) suggests a promising technique for investigating complex local cardiac events such as ''reentrant'' phenomenon using three-dimensional mapping techniques.[31]

## ACKNOWLEDGMENTS

This work was supported by a Richard A. and Nora Eccles Harrison Treadwell Fund for Cardiovascular Research and awards from the Nora Treadwell Foundation.

## REFERENCES

[1] Alfeld, P. Scattered data interpolation in three or more variables. In: Mathematical methods in CAGD, edited by T. Lyche and L. L. Schumaker. New York: Academic, 1989, pp. 1–33.
[2] Arisi, G., E. Macchi, S. Baruffi, S. Spaggiari, and B. Taccardi. Potential fields on the ventricular surface of the exposed dog heart during normal excitation. *Circ. Res.* 52:706–715, 1983.
[3] Arisi, G., E. Macchi, C. Corradi, R. L. Lux, and B. Taccardi. Epicardial excitation during ventricular pacing: Relative independence of breakthrough sites from excitation sequence in canine right ventricle. *Circ. Res.* 71:840–849, 1992.
[4] Barr, R. C., T. M. Gallie, and M. S. Spach. Automated production of contour maps for electrophysiology. I. Problem definition, solution strategy, and specification of geometric model. *Comput. Biomed. Res.* 13:142–153, 1980.
[5] Barr, R. C., and M. S. Spach. Sampling rates required for digital recording of intracellular and extracellular cardiac potentials. *Circulation* 55:40–48, 1977.
[6] Bayly, P. V., E. E. Johnson, S. F. Idriss, R. E. Ideker, and W. M. Smith. Efficient electrode spacing for examining spatial organization during ventricular fibrillation. *IEEE Trans. Biomed. Eng.* 40:1060–1066, 1993.
[7] Berbari, E. J., P. Lander, D. B. Geselowitz, B. J. Scherlag, and R. Lazzara. The methodology of cardiac mapping. In: Cardiac Mapping, edited by M. Shenasa, M. Borggrefe, and G. Breithardt. Armonk, NY: Futura, 1993, pp. 63–77.

[8] Berbari, E. J., P. Lander, B. J. Scherlag, R. Lazzara, and D. B. Geselowitz. Ambiguities of epicardial mapping. *J. Electrocardiol. Suppl.* 24, 16–20, 1991.

[9] Blanchard, S. M., R. J. Damiano, W. M. Smith, R. E. Ideker, and J. E. Lowe. Interpolating unipolar epicardial potentials from electrodes separated by increasing distances. *PACE* 12:1938–1955, 1989.

[10] Chen, P. S., P. D. Wolf, F. J. Claydon, E. G. Dixon, H. J. Vidaillet, N. D. Danieley, T. C. Pilkington, and R. E. Ideker. The potential gradient field created by epicardial defibrillation electrodes in dogs. *Circulation* 74:626–636, 1986.

[11] Ciaccio, E. J., A. L. Wit, M. M. Scheinman, S. M. Dunn, M. Akay, and J. Coromilas. Predication of the location and time of spontaneous termination of reentrant ventricular tachycardia for radiofrequency catheter ablation therapy. *J. Electrocardiol. Suppl.* 28:165–173, 1995.

[12] Colli Franzone, P., L. Guerri, and B. Taccardi. Spread of excitation in a myocardial volume: Simulation studies in a model of anisotropic ventricular muscle activated by point stimulation. *J. Cardiovasc. Electrophysiol.* 4:144–160, 1993.

[13] Downey, J. M. Why the endocardium? In: Therapeutic Approches to Myocardial Infarct Size Limitation, edited by D. J. Hearse and D. M. Yellon. New York: Raven, 1984, pp. 125–138.

[14] Farin, G. Smooth interpolation to scattered 3D data. In: Surfaces in Computer Aided Geometric Design. Amsterdam: North-Holland, 1983, pp. 43–63.

[15] Hodgkin, A. L., and A. F. Huxley. A quantitative description of membrane current and its application to conduction and excitation in nerve. *J. Physiol. (London)* 117:500–544, 1952.

[16] Ideker, R. E., W. M. Smith, S. M. Blanchard, S. L. Reiser, E. V. Simpson, P. D. Wolf, and N. D. Danieley. The assumptions of isochronal cardiac mapping. *PACE* 12:456–478, 1989.

[17] Idriss, S. F., S. B. Melnick, P. D. Wolf, W. M. Smith, and R. E. Ideker. Predicting the potential gradient field in ventricular fibrillation from shocks delivered in paced rhythm. *Am. J. Physiol.* 268:H2336–H2344, 1995.

[18] Janse, M. J., A. G. Kleber, A. Capucci, R. Coronel, and F. Wilms-Schopman. Electrophysiological basis for arrhythmias caused by acute ischemia: Role of subendocardium. *J. Mol. Cell. Cardiol.*, 18:339–355, 1986.

[19] MacLeod, R. S., and C. R. Johnson. Map3d: Interactive scientific visualization for bioengineering data. In: Proceedings of the IEEE Engineering in Medicine and Biology Society 15th Annual International Conference. New York: IEEE, 1993, pp. 30–31.

[20] MacLeod, R. S., R. L. Lux, and B. Taccardi. Translation of body surface maps between different electrode configurations using a three-dimensional interpolation scheme. In: Electrocardiology '93: Proceedings of the International Congress on Electrocardiology, XXth Annual Meeting, edited by P. W. MacFarlane. Singapore: World Scientific, 1993, pp. 179–182.

[21] Monro, D. M. Interpolation methods for surface mapping. *Comput. Program Biomed.* 11:145–157, 1980.

[22] Oostendorp, T. F., A. van Oosterom, and G. J. Huiskamp. Interpolation on a triangulated 3D surface. *J. Comput. Phys.* 80:331–343, 1989.

[23] Roberts, D. E., L. T. Hersh, and A. M. Scher. Influence of cardiac fiber orientation on wavefront voltage, conduction velocity, and tissue resistivity in the dog. *Circ. Res.* 44:701–712, 1979.

[24] Roberts, D. E., and A. M. Scher. Effect of tissue anisotropy on extracellular potential fields in canine myocardium *in situ*. *Circ. Res.* 50:342–351, 1982.

[25] Rudy, Y., and R. Plonsey. A comparison of volume conductor and source geometry on body surface and epicardial potentials. *Circ. Res.* 46:283–291, 1980.

[26] Savard, P., G. Bonneau, G. Tremblay, R. A. Leblanc, R. Cardinal, P. Pagé, and R. A. Nadeau. Interactive cardiac mapping system for antiarrhythmia surgery. In: IEEE Engineering in Medicine and Biology Society 8th Annual International Conference. New York: IEEE, 1986, pp. 1286–1288.

[27] Schijvenaars, B. J. A., J. A. Kors, G. van Herpen, F. Kornreich, and J. H. van Bemmel. Interpolation of body surface potential maps. *J. Electrocardiol. Suppl.* 28:104–109, 1996.

[28] Spach, M. S., and P. C. Dolber. Relating extracellular potentials and their derivatives to anisotropic propagation at a microscopic level in human cardiac muscle. *Circ. Res.* 58:356–371, 1986.

[29] Spach, M. S., P. C. Dolber, and J. F. Heidlage. Influence of the passive anisotropic properties on directional differences in propagation following modification of the sodium conductance in human atrial muscle: A model of reentry based on anisotropic discontinuous propagation. *Circ. Res.* 62:811–832, 1988.

[30] Spach, M. S., W. T. Miller, D. B. Geselowitz, R. C. Barr, J. M. Kootsey, and E. A. Johnson. The discontinuous nature of propagation in normal canine cardiac muscle: Evidence for recurrent discontinuities of intracellular resistance that affect the membrane currents. *Circ. Res.* 48:39–54, 1981.

[31] Taccardi, B., R. L. Lux, P. R. Ershler, R. S. Macleod, C. Zabawa, and Y. Vyhmeister. Potential distributions and excitation time maps recorded with high spatial resolution from the entire ventricular surface of exposed dog hearts. In: Computers in Cardiology. Los Alamitos, CA: IEEE Computer Press, 1992, pp. 1–4.

[32] Taccardi, B., E. Macchi, R. L. Lux, P. R. Ershler, S. Spaggiari, S. Baruffi, and Y. Vyhmeister. Effect of myocardial fiber direction on epicardial potentials. *Circulation* 90:3076–3090, 1994.